AJNR

Three-dimensional gradient-recalled MR imaging as a screening tool for the diagnosis of cervical radiculopathy.

J S Tsuruda, D Norman, W Dillon, T H Newton and D G Mills

AJNR Am J Neuroradiol 1989, 10 (6) 1263-1271
http://www.ajnr.org/content/10/6/1263

Three-Dimensional Gradient-Recalled MR Imaging as a Screening Tool for the Diagnosis of Cervical Radiculopathy

Jay S. Tsuruda[1]
David Norman[1]
William Dillon[1]
T. Hans Newton[1]
Don G. Mills[2]

The purpose of the study was to implement and assess a fast-screening, three-dimensional Fourier transformation (3DFT) MR sequence for the cervical spine. This sequence maintains adequate signal-to-noise and image contrast similar to gradient-recalled echo two-dimensional Fourier transformation (2DFT) imaging. Thirty patients with radiculopathy were examined with 3DFT gradient-recalled echo imaging. The data set consisted of 60 contiguous 1.5- to 2.0-mm-thick axial slices with a total coverage of 9 to 12 cm. In 10 patients, comparison was made with 4-mm-thick axial T1-weighted spin-echo 2DFT or gradient-recalled echo 2DFT studies. With the use of a volume acquisition, adequate signal-to-noise and image contrast similar to T2*-weighted gradient-recalled echo 2DFT acquisitions were obtainable. Coverage was improved despite the use of thinner sections without interslice gap. Thin-section 3DFT provided superior detail of acquired foraminal and spinal canal stenosis and disk morphology. Limitations included increased sensitivity to patient motion and "wraparound" artifact in the slice-select direction.

Overall, diagnostic confidence was improved with 3DFT owing to the reduction of partial volume artifact. We have adopted this technique as the primary screening method for diagnosing cervical radiculopathy.

***AJNR* 10:1263–1271, November/December 1989; *AJR* 154: February 1990**

MR imaging with surface coils is currently the preferred method for evaluating degenerative cervical spine disease. In prospective and retrospective studies, both short and long TR spin-echo images of the cervical spine have shown a high degree of correlation compared with myelography, CT, CT myelography, and surgical findings [1, 2]. However, several disadvantages have retarded the use of MR as a screening method for degenerative disease of the cervical spine. These include the inability to obtain sections less than 3- to 5-mm thick, resulting in partial volume averaging and suboptimal differentiation between osteophytes and disk material. Herniated disks extending into the obliquely oriented lateral root canals are not as reliably identified as on intrathecal contrast CT with 1.5-mm-thick sections [1]. Inadequate image contrast between bone and soft tissue may diminish MR specificity [2]. Motion artifact associated with prolonged acquisition times may prevent diagnostic utility.

With the development of short TR, gradient-recalled echo (GRE) techniques, cervical spine images with enhanced CSF signal intensity can be obtained rapidly [3–6]. An overall improvement in depicting degenerative disease of the cervical spine including disk herniation, osteophytes, foraminal stenosis, and narrowing of the subarachnoid space has been noted [7]. A recent study correlated spin-echo and gradient-echo acquisitions with anatomic sections [8]. T2*- or proton-density-weighted gradient-echo images were found to be superior to spin-echo images in depicting the soft-tissue contents and bone margins of the cervical neural foramina

Received January 19, 1989; revision requested March 30, 1989; revision received April 18, 1989; accepted April 25, 1989.

Presented at the annual meeting of the American Society of Neuroradiology, Orlando, March 1989.

[1] Department of Radiology, Diagnostic and Interventional Neuroradiology Section, University of California, San Francisco, 505 Parnassus Ave., San Francisco, CA 94143. Address reprint requests to J. S. Tsuruda.

[2] Diagnostic Imaging Consultants, Inc., Chattanooga, TN 37404.

0195-6108/89/1006–1263

and in estimating foraminal size. Because of these advantages, this technique may be "the initial procedure of choice for the evaluation of suspected cervical radiculopathy" [9]. Despite the improvement in image contrast and the decrease in imaging times with the GRE techniques, limitations in minimum slice thickness inherent to two-dimensional Fourier transformation (2DFT) images remain.

Three-dimensional Fourier transformation (3DFT) imaging provides several advantages over 2DFT GRE studies. These advantages include the ability to obtain very thin contiguous slices and improvement of signal-to-noise and spatial resolution. In addition, an isotropic voxel data set can be obtained so that retrospective reconstruction and motion-artifact suppression can be employed [9–14]. In the past, 3DFT was not feasible for routine use with conventional spin-echo techniques because of the long acquisition times, especially if T2-weighted images were desired [15–18]. More recently, fast-scanning techniques have reduced this time. For these reasons 3DFT evaluation of the knee [19, 20] and temporomandibular joint [21] has gained clinical importance. Our goal was to implement and assess a fast, thin-section 3DFT sequence for the cervical spine while maintaining adequate signal-to-noise and image contrast similar to gradient-recalled 2DFT imaging.

Material and Methods

Thirty patients were referred to MR for the initial evaluation of cervical radiculopathy. MR was performed at 1.5 T.* All patients were studied in a supine neutral position with a flat 5-in. planar dorsal GE surface coil. In a minority of studies, self-shielded RF gradient coils were used.

All patients were studied initially with two sequences in the sagittal plane with multislice, 2DFT techniques. First, a T2*-weighted multiplanar gradient-recalled (MPGR) GRE acquisition was obtained as a localizing study using 500/20/2 (TR/TE/excitations), a flip angle of 20°, field of view of 24 cm, slice thickness of 4 mm, interslice gap of 0 mm, matrix of 256 × 192, imaging time of 3:19 min, and a total of 14 slices. This was followed by a T1-weighted spin-echo acquisition using 600/20/4, a field of view of 24 cm, slice thickness of 3 mm, interslice gap of 1 mm, matrix of 256 × 256, imaging time of 10:17 min, and a total of 11 slices. Motion artifact was diminished with gradient-moment nulling (flow compensation) [22] on the GRE study and with the application of a 12-cm-thick saturation RF pulse [23] over the anterior soft tissues of the neck on the T1-weighted sequence. Gradient-moment nulling was not used with the T1-weighted sequence in order to maintain a minimum TE value.

After the sagittal images were obtained, a 3DFT GRE study was performed [10, 24]. A diagrammatic representation of this sequence is shown in Figure 1. A selective RF pulse combined with a gradient in the slice-select direction was used to excite a large volume or slab in the neck. Spatial resolution in the frequency-encoding direction (G_x) was acquired by the application of a gradient reversal, which also generated a gradient-refocused echo. Spatial resolution in the other two directions was obtained by the use of two phase-encoding gradients (G_z and G_y), which were oriented perpendicular to each other. In all cases, the slice-selection direction (G_z) was oriented in the superior-inferior direction. Therefore, after data reconstruction

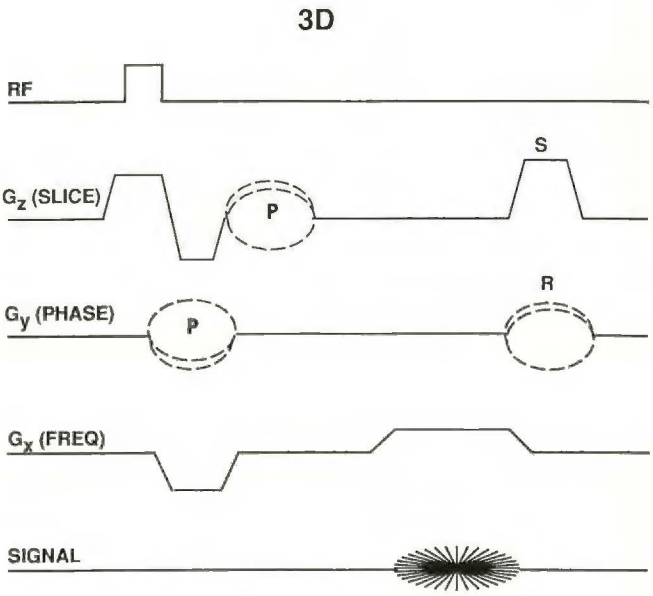

Fig. 1.—Schematic diagram for 3DFT gradient-recalled echo MR imaging. A slab of tissue is excited by a selective 5° RF pulse combined with a gradient in the slice-select direction (G_z). Two phase-encoding gradients (P) are applied in two directions (G_z and G_y). A gradient-recalled echo is generated by gradient reversal in the frequency-encoding (G_x) axis. The signal is processed by 3DFT to yield the final image. A rewinding or refocusing pulse (R) is used to rephase in-plane transverse magnetization after it is measured and prior to the next RF pulse. At the same time, a nonvariable spoiler gradient (S) is used to destroy any unwanted phase buildup along the slice-select direction, which may cause artifactual misregistration of signal between adjacent slices. (Adapted from [24].)

with 3DFT, the primary plane of section was axial. Within the plane of section, G_x and G_y were oriented in the right-to-left and anterior-posterior directions, respectively. Following the gradient echo, a rewinding or refocusing pulse was applied in the G_y axis and a generalized spoiler gradient was used in the G_z direction. Gradient-moment nulling was used in all cases; however, this is not shown in Figure 1 for the sake of simplicity.

The 3DFT GRE parameters were: 35/15/2, flip angle 5°, field of view 20 cm, slice thickness 1.5–2.0 mm, interslice gap 0 mm, matrix 256 × 128, 64 slices, and imaging time 9:34 min. Voxels were anisotropic with a volume ranging between 1.8 and 2.4 cubic mm for 1.5- and 2.0-mm-thick slices, respectively.

In 10 patients, additional axial images were obtained with either a multislice (MPGR) T2*-weighted GRE or T1-weighted spin-echo 2DFT sequence. Parameters for the MPGR sequence were 600/20/4, flip angle 15°, field of view 24 cm, slice thickness 4 mm, interslice gap 0 mm, matrix 256 × 192, gradient-moment nulling, 17 slices, and imaging time 7:44 min. The spin-echo sequence parameters were 800/20/4, field of view 20 cm, slice thickness 4 mm, interslice gap 1 mm, matrix 256 × 192, 15 slices, and imaging time 10:14 min. Saturation RF pulses were applied superiorly, anteriorly, and inferiorly outside the imaging volume during the spin-echo sequence to diminish motion and entry-slice artifact from pulsatile CSF and vascular motion. Comparisons between the various axial techniques were made in a nonblinded fashion for overall image quality, the presence of artifacts, and visualization of osseous and soft-tissue detail. On both the 2DFT and 3DFT GRE studies, CSF signal intensity was compared with cord intensity by using a numerical score based on a previously established scale [25] as follows: 1 = CSF isointense and indistinguishable from

* Signa, software version 3.2 Beta and Performance Plus, General Electric Company, Milwaukee, WI.

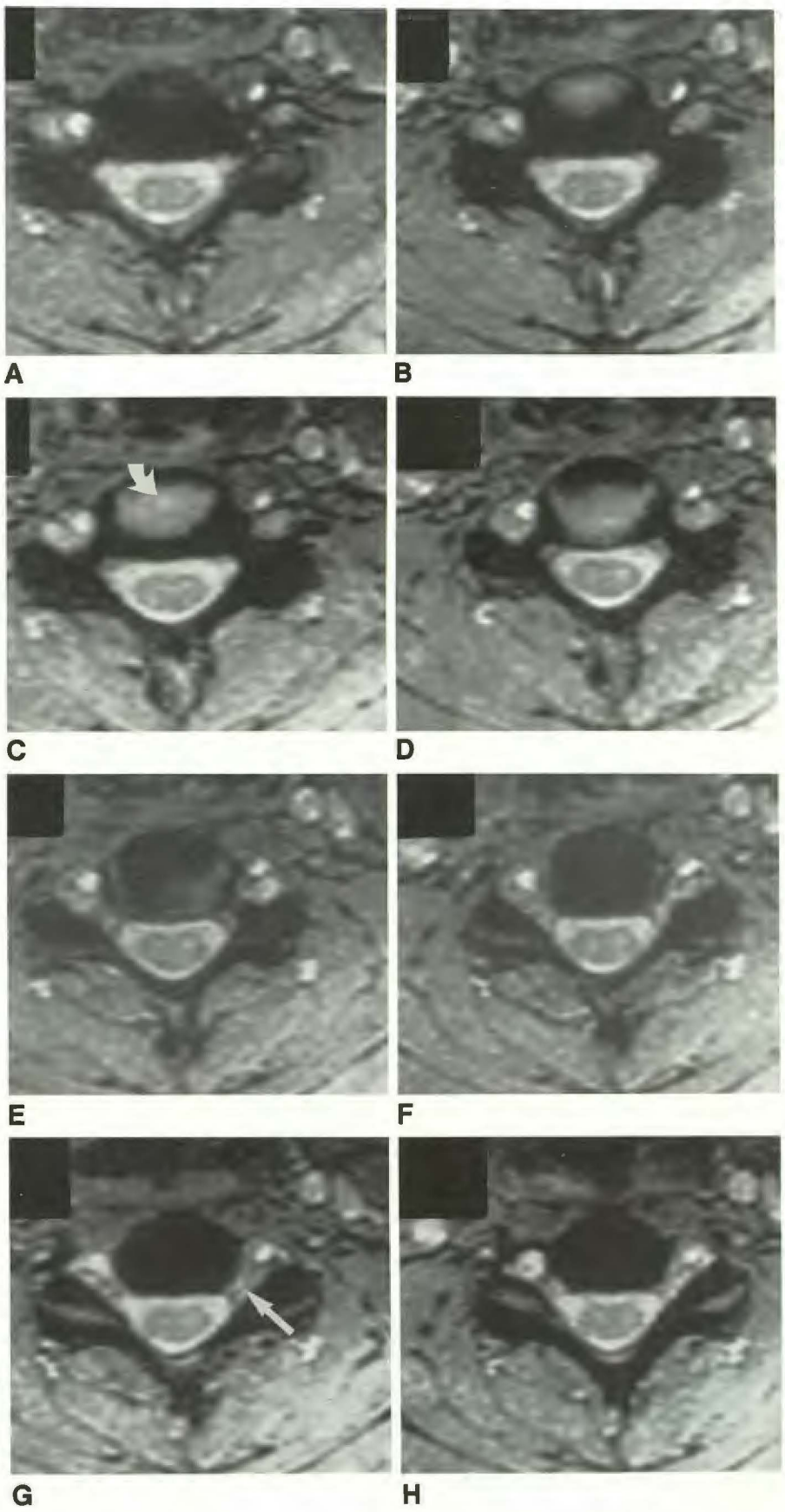

Fig. 2.—*A–H*, Normal 3DFT examination through the C5–C6 level. Images are depicted from the most caudal (*A*) to rostral (*H*) level. High-signal-intensity CSF relative to the lower-intensity cord and bone is evident. Clear definition of the neural foramina (*straight arrow* in *G*) and intervertebral disk (*curved arrow* in C) is obtained with the use of 1.5-mm sections.

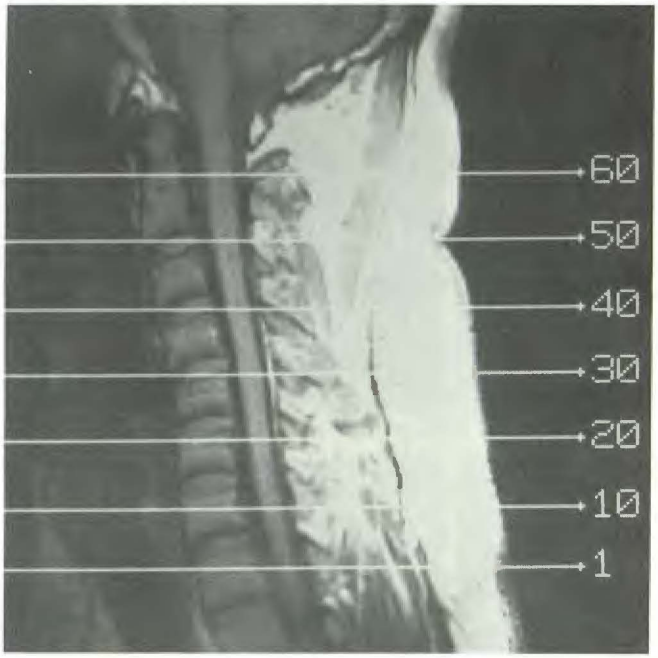

Fig. 3.—Mid-sagittal T1-weighted image shows slice positions and overall coverage for a single 60-slice 3DFT acquisition with 2-mm-thick sections. The levels corresponding to each 10th slice are shown. Note signal drop-off in anterior soft tissues of neck caused by the application of a broad saturation RF pulse.

cord, 2 = CSF slightly higher than cord, 3 = high-signal CSF with indistinct cord contour, 4 = high-signal CSF with sharply defined cord margins.

Results

An example of normal anatomy obtained with 3DFT GRE is shown in Figure 2. In Figure 3, the 3DFT axial slice positions are shown along with the mid-sagittal image from a T1-weighted acquisition in a different patient. The coverage [26] (no. of slices × slice thickness) ranged from 9.0 to 12.0 cm for the 1.5- and 2.0-mm-thick slices, respectively. By comparison, the coverage for the 2DFT GRE sequence was limited to 6.8 cm despite the use of thicker slices. Intervertebral disks and neural foraminal soft tissue have a high signal intensity in contrast to very low signal intensity of bone [7–9, 25]. Examples of a left paracentral disk protrusion (Fig. 4) and intraforaminal disk herniation (Fig. 5) are shown.

2DFT GRE was equivalent to 3DFT GRE in the identification of acquired foraminal stenosis due to osseous hypertrophy. However, in all cases the thinner slice sections available on the 3DFT studies provided greater detail of the degree of encroachment on the neural foramina (Fig. 6). Cord displacement was seen equally well with both techniques. Both 2DFT and 3DFT GRE sequences were superior to T1-weighted axial images in their ability to identify degenerative changes.

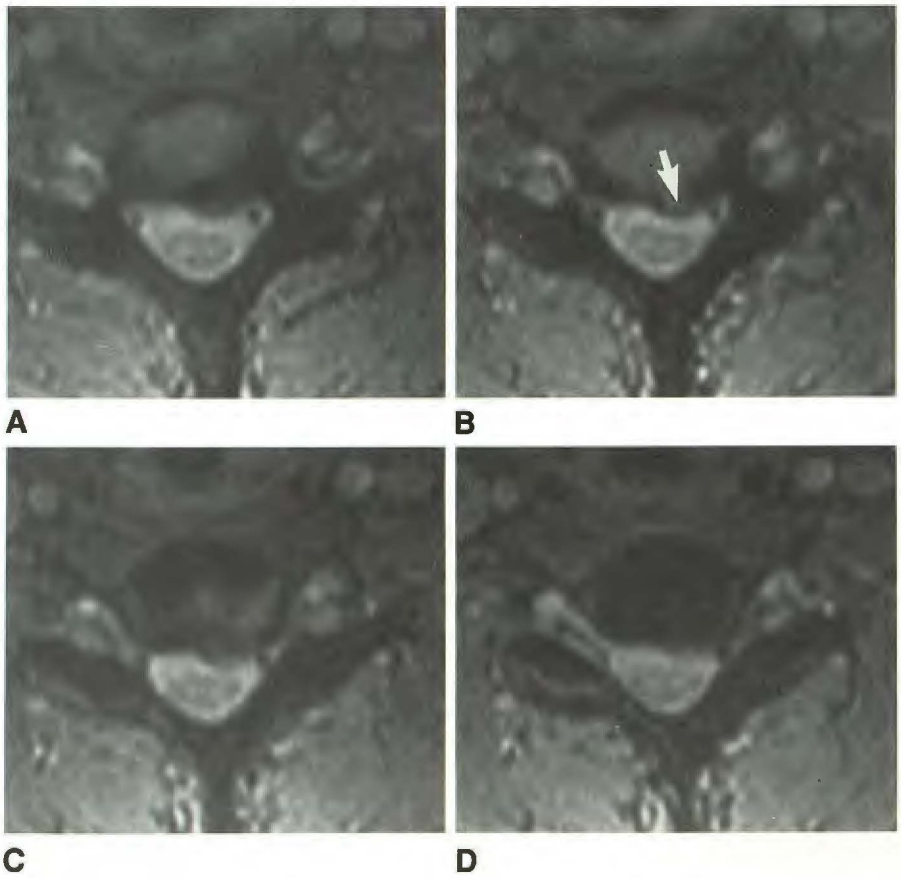

Fig. 4.—*A–D*, C6–C7 disk protrusion shown by 3DFT gradient-recalled echo. *Arrow* in *B* indicates a left paracentral disk protrusion with intermediate signal intensity adjacent to hyperintense CSF. The adjacent cervical cord is deformed.

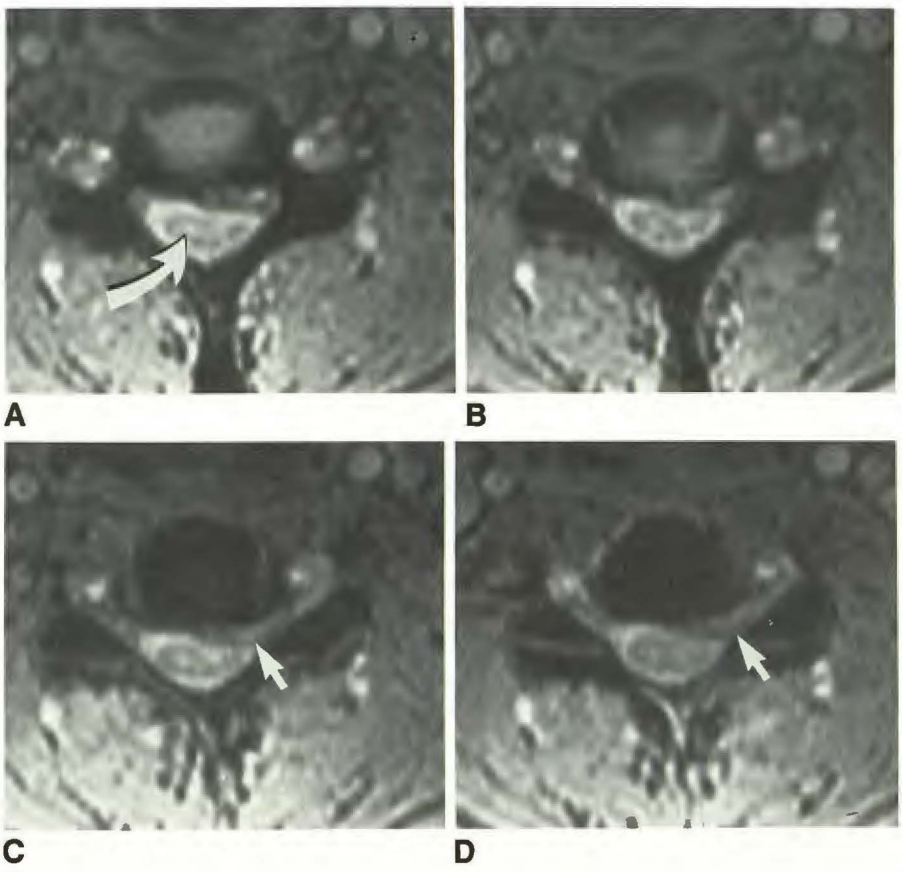

Fig. 5.—*A–D*, Intraforaminal disk herniation shown by 3DFT gradient-recalled echo. *Short arrow* in *C* and *D* indicates intermediate-intensity disk material extending into left C5–C6 neural foramen. Compression of cord is present. Truncation artifact, represented by a band of intramedullary hyperintensity (*curved arrow* in *A*), is seen.

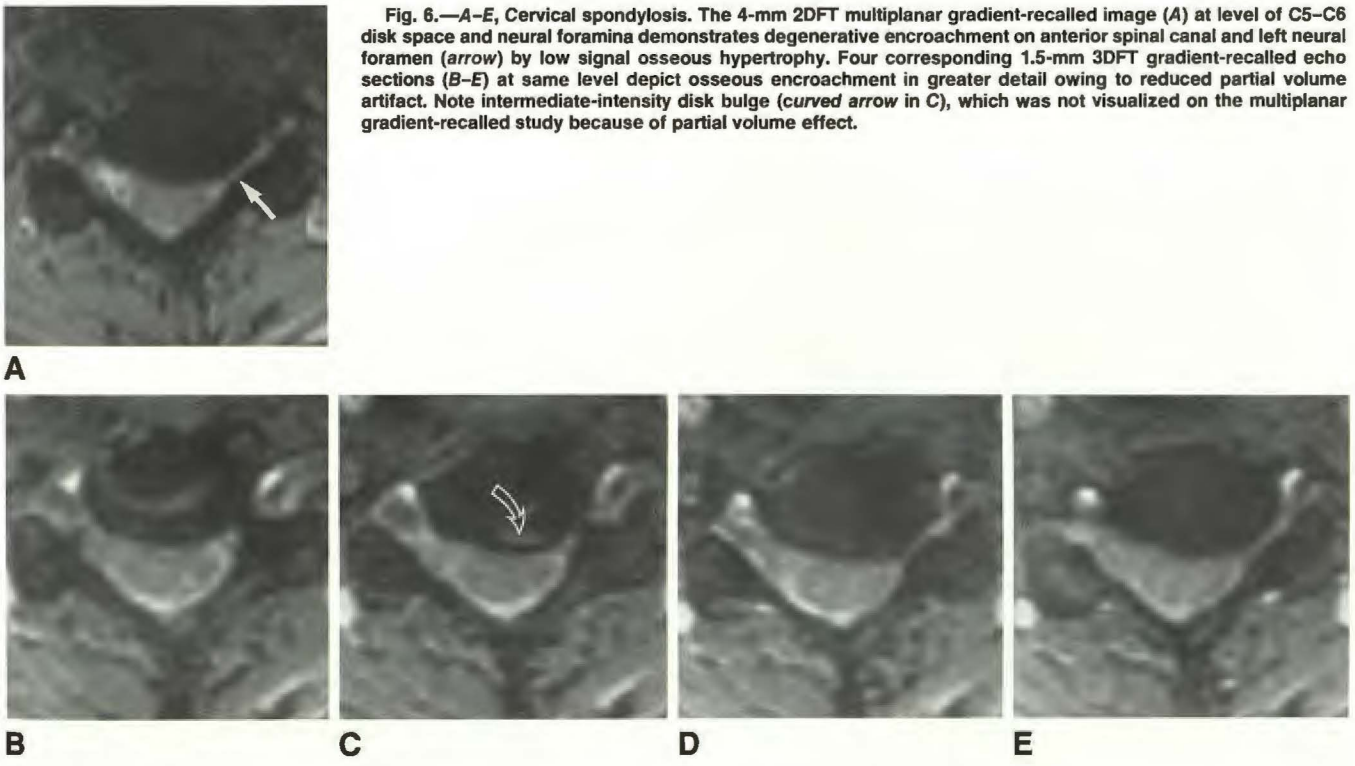

Fig. 6.—*A–E*, Cervical spondylosis. The 4-mm 2DFT multiplanar gradient-recalled image (*A*) at level of C5–C6 disk space and neural foramina demonstrates degenerative encroachment on anterior spinal canal and left neural foramen (*arrow*) by low signal osseous hypertrophy. Four corresponding 1.5-mm 3DFT gradient-recalled echo sections (*B–E*) at same level depict osseous encroachment in greater detail owing to reduced partial volume artifact. Note intermediate-intensity disk bulge (*curved arrow* in *C*), which was not visualized on the multiplanar gradient-recalled study because of partial volume effect.

The overall image contrast with relatively high CSF signal compared with cord intensity was comparable to the findings previously demonstrated with either single or multislice 2DFT GRE axial images [7, 9]. In all cases, the CSF signal was equal to or greater than intensity of the cord, with 67% of the cases rated between 3 and 4. Of the 3DFT studies, 15% were determined to be technically inadequate owing to poor contrast distinction between CSF and cord. Suboptimal quality was caused by motion artifact, resulting in image degradation, severe spondylosis with compression of the thecal sac, and aliasing in the slice-select direction (Fig. 7). Significant artifactual heterogeneity of signal intensity was noted within the cord in 30% of the cases (Fig. 5). This finding was presumably caused by truncation artifact, since such heterogeneity was not noted on the 2DFT sagittal sequences [27].

In 41% of the patients, self-shielded RF gradient coils were used to acquire the images. A slight improvement in image quality, characterized by sharper soft tissue and osseous boundaries and improved CSF-to-cord contrast, was noted.

Discussion

MR imaging has proved to be an important screening technique for the evaluation of cervical radiculopathy. The commonly used axial 2DFT T1-weighted spin-echo images have limitations, of which the most important is poor contrast resolution among osteophytes, CSF, ligaments, and dura, all of which have similar low signal intensity [25]. Gd-DTPA–enhanced T1-weighted images enhance soft-tissue detail in the neural foramina, allowing improved detection of foraminal encroachment [8]. Gd-DTPA was not used in our patients, since our goal was to establish a noninvasive screening sequence. T1-weighted spin-echo techniques also have limited coverage. In multilevel disease, additional scan time is required, so patient discomfort may be prolonged. Axial T2-weighted spin-echo images with or without cardiac gating have limited usefulness because of CSF pulsatile artifacts [25].

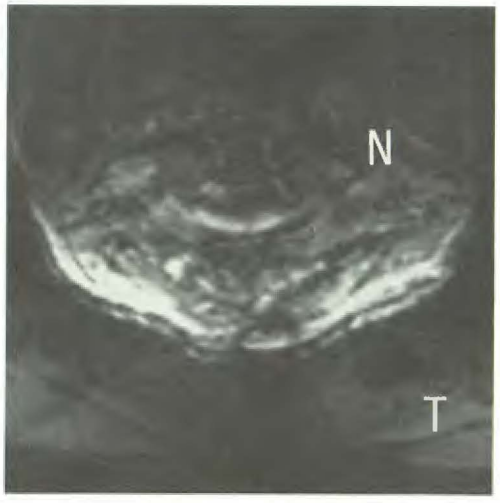

Fig. 7.—Aliasing artifact in the slice-select direction. The lowest 3DFT axial section through T2 level (T) is degraded by superimposition of an axial image of the upper neck (N). See Discussion section for explanation.

Proton-density- or T2*-weighted 2DFT GRE techniques have improved detection of degenerative extradural defects [7–9, 25]. Signal-to-noise limitations often require an increase in the number of excitations or in the slice thickness. These factors result in prolongated scan time or increases in partial volume averaging. Signal-to-noise is a limiting factor in single-slice GRE techniques. This limitation is circumvented with multisection GRE techniques with TR between 500–1000 msec [28]. Coverage is greater since many slices are excited during each TR interval. Clinical trials of multisection GRE of the cervical spine have demonstrated its advantage over T1-weighted images [7, 8], and is one of the comparative techniques used in this study.

Slice thickness must approximate that of CT for an MR protocol to have equivalent sensitivity as a screening technique for the cervical spine. We have noted that undesirable patient motion increases with acquisition times that exceed 10 min. Therefore, a reasonably short scan time is also important. Signal-to-noise, resolution, coverage, image contrast, and artifact suppression must also be considered. In this regard, 3DFT GRE imaging may offer some advantages.

Although 2DFT GRE improves image contrast, partial volume artifact continues to be a limiting factor because of the minimal slice thickness limitation of all 2DFT techniques. Slice thickness is proportional to the bandwidth of the RF pulse and inversely proportional to the gradient amplitude in the slice-select direction [29]. Hardware limitations on our current system hold the minimum slice thickness to 3 mm. This slice thickness corresponds to a minimum bandwidth of 1.25 kHz and a maximum gradient strength of 1 G/cm. A further reduction in bandwidth will lengthen the RF pulse and prolong the minimum TE, resulting in a reduction in signal-to-noise [29]. Increases in the gradient strength are limited by the gradient power supply. By comparison, slice thickness with 3DFT is independent of RF bandwidth and is inversely proportional to the duration of the phase-encoding gradient [30]. Thus, thinner sections are acquired by increasing the time the phase-encoding gradient is on. A stronger slice-selection gradient is not required. The thinnest section currently available on our scanner is 0.7 mm.

Slice profile with 2DFT imaging is dependent on an RF sinc pulse in the presence of a gradient, which may introduce cross talk. The introduction of an interslice gap will reduce this phenomenon but introduces partial volume artifact [26, 31]. In 3DFT reconstruction, a phase-encoding gradient determines the section profiles following the same rules as in-plane resolution [18]. Contiguous slices are therefore possible. The total number of slices is a function of the number of phase-encoding projections. Additionally, the total number of slices, unlike 2DFT imaging, is independent of TR. Cross talk between slices, resulting from truncation artifact, can also occur with 3DFT techniques [32], as discussed below.

Adequate signal-to-noise must be maintained as slice thickness is reduced. 3DFT offers the advantage that a second phase-encoding gradient is required for slice selection [14]. The signal-to-noise improves as the square root of the number of additional phase projections, which is equal to the number of slices. This gain in signal comes as a penalty in acquisition time, since the total imaging time (T) is given as

$$T = Nsl \cdot Npl \cdot TR \cdot NEX$$

where *N*sl and *N*pl are the number of phase projections in the slice and in-plane phase-encoding directions [11]. Relative improvements in signal-to-noise in 2DFT and 3DFT techniques must be assessed on a per unit time basis. Signal-to-noise improvement per unit time is most efficient in routine 2DFT spin-echo imaging with relatively long TRs. However, advantages in signal-to-noise can also be associated with 3DFT imaging by using short TR, GRE sequences [32].

Since total imaging time is a product of an additional phase-encoding gradient, the use of long TR spin-echo 3DFT sequences for either T1- or T2-weighted images would be prohibitive in spine imaging, especially if multiple slices are required. One study took 61 min to acquire a 3DFT T1-weighted examination (TR = 300, 64 slices) of the lumbar spine [18]. In an attempt to shorten the imaging time, the TR was set at 35 msec.

An added advantage of a short TR is its beneficial effect on image contrast by enhancing CSF signal intensity. When TR is less than the transverse relaxation time, T2, steady-state transverse magnetization is established [5, 33–36]. This residual transverse magnetization is not destroyed between phase-encoding cycles, and image contrast is strongly influenced by T1 and T2. A refocusing pulse in the Gy axis is applied that incorporates this transverse coherence so that tissues with a longer T2 have relatively greater signal intensity (Fig. 1). Since the calculated T2 of CSF is greater than gray or white matter (396 vs 57–69 msec), a "myelographic" effect can be obtained [5]. The use of a short TR combined with refocusing gradients will boost the signal per unit time compared with sequences using a longer TR [36].

The above assumptions require that steady state free precession (SSFP) be present. This holds true for stationary CSF. With refocused short TR 2DFT GRE, calculated contrast curves have demonstrated that higher signal can be generated by CSF in comparison with either gray or white matter by increasing the flip angle, with the greatest differences between 50–90° [5, 36, 37]. In reality, this does not occur in cervical spine imaging, since CSF is not stationary [25]. Moving CSF results in a non-SSFP state, and positive contrast, based on proton-density differences, only occurs with very low flip angles with a crossover point at 10°. A rapid decline in pulsatile CSF signal intensity occurs with higher flip angles [37]. To achieve this contrast effect, we selected a 5° flip angle knowing that this was a compromise, since overall signal intensity drops precipitously with low flip angles [36]. Cardiac gating may assist in establishing SSFP; this option was not available to us and is probably impractical, as total imaging time may be lengthened since data acquisition might only occur during diastole.

Because of our desire for image contrast yielding a "myelographic" effect, the reduced signal-to-noise influenced the limits of resolution. With 3DFT imaging, the theoretical resolution can be equal in all three directions, thus yielding small isotropic voxels, for example 1.0 cubic mm. Retrospective, multiplanar reformations and surface reconstruction such as in the knee [16] or lumbar spine [18] is then possible. The use of isotropic techniques in the cervical spine resulted in poor signal-to-noise unless the imaging time was unduly prolonged. Since reformation algorithms are not readily available for our system, the voxel size was increased to 1.8–2.4 cubic mm to increase signal intensity and the axial plane was used as the primary plane of reconstruction. In-plane resolution (1.56 × 0.78 mm) was thought to be adequate although it is slightly less than the comparison 2DFT techniques used in this study. A benefit of a larger voxel is the expanded coverage [26].

It would be desirable for a screening examination of the cervical spine to cover C3 through T1 levels corresponding to 8–9 cm in an adult patient. With our 2DFT techniques, coverage was limited to 6.8 and 6.0 cm for the GRE and T1-weighted sequences, respectively. This limitation occasionally required the placement of a limited number of slices at each disk space using a sagittal localizer as a guide in patients with extensive, multilevel degenerative disease. By comparison, the coverage of the 3DFT technique ranged between 9.0 and 12.0 cm (Fig. 2). This simplified the examination for the technologist, since precise localization of a limited set of axial images was not required.

Artifacts caused by motion, magnetic susceptibility, and truncation occur with both 2DFT and 3DFT techniques. Image degradation resulting from motion appears to be greater with 3DFT, presumably because of the application of an additional phase-encoding gradient. As a result, phase ghosting in two axes that are perpendicular to each other can occur. Since motion artifact is commonly due to swallowing or vascular pulsation in the anterior tissues of the neck, a dorsal surface coil was used to reduce signal from this area. Unfortunately, saturation pulses similar to those used for 2DFT imaging (Fig. 2) were not available for 3DFT imaging. It is experimentally possible to reduce motion artifact in anesthetized small animals by 3DFT GRE imaging by using signal averaging to offset periodic respiratory and vascular motion [13]. Motion suppression did not occur in our patients, probably because of the nonperiodic nature of the patient motion.

Magnetic susceptibility has been documented in vitro [38] and in vivo in the brain [39] and cervical spine [40]. This artifact is generated whenever spatial variation in the induced magnetic field results in geometric distortion. It is more apparent on GRE images and is directly proportional to the TE and inversely proportional to the spatial resolution [31, 41]. In the cervical spine, this artifact may accentuate or mimic foraminal stenosis and appear similar to osseous or ligamentous encroachment on the spinal canal [40]. This artifact can be reduced by reducing the TE to its minimum value. In this study, the minimum TE was 15 msec. Shorter TEs are possible if gradient moment nulling is eliminated [42]; however, we found that this resulted in unacceptable motion artifact. Magnetic susceptibility can be reduced by increasing spatial resolution (decreasing voxel size). Since magnetic susceptibility will increase with increasing intrinsic magnetic field gradients across imaging voxels [40], reduction of voxel size will lessen this effect [41]. From a practical standpoint, 3DFT can achieve smaller voxel dimensions. Qualitatively, we did not notice significant susceptibility artifacts with 3DFT GRE imaging when using the stated parameters. Quantitative evaluation is required.

MR truncation artifact [27] is most evident along the phase-encoding axis between regions that are markedly dissimilar in signal intensity [43]. In cross-sectional cervical spine imaging, this artifact is manifested as heterogeneous bands of signal intensity, and increases with reduction of the in-plane phase-encoding matrix to 128. We have noted similar findings in some of our cases since a 128 matrix was used to reduce scan time (Fig. 5). Therefore, this technique is not applicable for screening of intramedullary disease. With 3DFT imaging, truncation could also occur between adjacent slices because of the orientation of the second phase-encoding gradient, resulting in cross talk, which can be minimized when slice thickness is less than 3 mm [32].

Eddy current, generated by the interaction of the RF coils with the other components of the magnet including the cryostat and shim coils, could cause significant distortion of the gradient field and current waveform. Eddy currents will alter image quality by causing spatial distortion and shading in the images [44]. Correction can be achieved by using self-shielded coils [45]. We noted a qualitative overall improvement in image quality with these coils with sharper boundaries between bone, cord, and CSF margins.

Finally, because of the method of data collection with 3DFT, unique artifacts can be generated that have not been seen with 2DFT techniques. Aliasing or phase wrap is a well-known artifact that occurs when an object outside the field of view is spatially mismapped into the region of interest. On cross-sectional 2DFT imaging, this artifact is seen along the phase-encoding direction. Since 3DFT incorporates a second phase gradient along the slice-select direction, aliasing can occur perpendicular to the slice profile direction because of tissue that is partially excited outside the imaging volume (Fig. 7). Since the degree of excitation diminished rapidly from the region of interest, aliasing is greatest in the outer sections [11]. In our imaging protocol, the first two slices at each end of the 64-slice study were discarded and only the center 60 images were displayed. Minimal residual aliasing artifact was persistent in the remaining end slices and was greatest in the cervical-thoracic junction. In a minority of patients (10%) there was significant image degradation of the C7–T1 interspace. In the remainder of the patients, aliasing was outside the most important region of interest.

The observations discussed above point to a rational basis for the use of 3DFT GRE techniques in screening for cervical radiculopathy. As with 2DFT imaging, compromises between imaging time, signal-to-noise, resolution, image contrast, and coverage need to be considered when devising an imaging protocol. The major advantages with this technique are the ability to obtain very thin, contiguous sections with reduction of partial volume averaging with preservation of image contrast similar to T2*-weighted 2DFT GRE images. This volumetric acquisition provides excellent coverage and is time-efficient. Artifacts peculiar to 3DFT may be a limiting factor. No systematic attempt was made to correlate the imaging results with either the surgical findings or clinical symptoms. In this regard, this study is incomplete, and, ultimately, a carefully designed prospective trial is required to validate our findings.

REFERENCES

1. Brown BM, Schwartz RH, Frank E, Blank NK. Preoperative evaluation of cervical radiculopathy by surface-coil MR imaging. *AJNR* **1988**;9:859–866, *AJR* **1988**;151:1205–1212
2. Modic MT, Masaryk TJ, Mulopulos GP, Bundschun CV, Han JS, Bohlman H. Cervical radiculopathy: prospective evaluation with surface coil MR imaging, CT with metrizamide, and metrizamide myelography. *Radiology* **1986**;161:753–759
3. Buxton RB, Edelman RR, Rosen BR, Wismer GL, Brady TJ. Contrast in rapid MR imaging: T1- and T2-weighting. *J Comput Assist Tomogr* **1987**; 11:7–16
4. Mills TC, Ortendahl DA, Hylton NM, Crooks LE, Carlson JW, Kaufman L. Partial flip angle imaging. *Radiology* **1987**;162:531–539
5. Perkins TG, Wehrli FW. CSF signal enhancement in short TR gradient echo images. *Magn Reson Imaging* **1986**;4:465–467
6. Young IR, Payne JA, Collins AG, Bydder GM. MRI: the development of T1 contrast with rapid field echo sequences. *Magn Reson Med* **1987**;4: 333–340
7. Kulkarni MC, Narayana PA, McCardle CB, Yeakley JW, Campagna NF, Wehrli FW. Cervical spine MR imaging using multislice gradient echo imaging: comparison with cardiac gated spin echo. *Magn Reson Imaging* **1988**;6:517–525
8. Czervionke LF, Daniels DL, Ho PS, et al. Cervical neural foramina: correlative anatomic and MR imaging study. *Radiology* **1988**;169:753–759
9. Hedberg MC, Drayer BP, Flom RA, Hodak JA, Bird CR. Gradient echo (GRASS) MR imaging in cervical radiculopathy. *AJNR* **1988**;9:145–151
10. Frahm J, Haase A, Matthaei D. Rapid three-dimensional MR imaging using the FLASH technique. *J Comput Assist Tomogr* **1986**;10:363–368
11. Johnston G, Hutchinson JMS, Redpath TW, Eastwood LM. Improvements in performance time for simultaneous three-dimensional imaging. *J Magn Reson Imaging* **1983**;54:374–384
12. Kumar A, Welti D, Ernst RR. NMR Fourier zeugmatomagraphy. *J Magn Reson* **1975**;18:69–85
13. Matthaei D, Fram J, Haase A, Hanicke W, Merboldt K-D. Three-dimensional FLASH MR imaging of the thorax and abdomen without triggering or gating. *Magn Reson Imaging* **1986**;4:381–386
14. Pykett IL, Buonanno FS, Brady TJ, Kistler JP. Techniques and approaches to proton NMR imaging of the head. *Comput Radiol* **1983**;7:1–17
15. Gallimore GW, Harms SE. Selective three-dimensional MR imaging of the spine. *J Comput Assist Tomogr* **1987**;11:124–128
16. Harms SE, Muschler G. Three-dimensional MR imaging of the knee using surface coils. *J Comput Assist Tomogr* **1986**;10:773–777
17. Pykett IL, Buonanno FS, Brady TJ, Kistler JP. True three-dimensional nuclear magnetic resonance imaging in ischemic stroke: correlation of NMR, X-ray CT and pathology. *Stroke* **1983**; 14:173–177
18. Sherry CS, Harms S, McCroskey WK. Spinal MR imaging: multiplanar representation from a single high resolution 3D acquisition. *J Comput Assist Tomogr* **1987**;11:859–862
19. Spritzer CE, Vogler JB, Martinez S, et al. MR imaging of the knee: preliminary results with a 3DFT GRASS pulse sequence. *AJR* **1988**; 150:597–603
20. Tyrrell RL, Gluckert K, Pathria M, Modic MT. Fast three-dimensional MR imaging of the knee: comparison with arthroscopy. *Radiology* **1988**;166: 865–872
21. Wilk RM, Harms SE. Temporomandibular joint: multislab, three-dimensional Fourier transformation MR imaging. *Radiology* **1988**;167:861–863
22. Quencer RM, Hinks RS, Pattany PH, Horen M, Donovan Post MJ. Improved MR imaging of the brain by using compensating gradients to suppress motion-induced artifacts. *AJNR* **1988**;9:415–424
23. Ehman RL, Felmlee JP, Berquist TH, Julsrud PR, Gray JE. Clinical trial of a spatial presaturation technique for reducing flow and motion artifacts in MR images: comparison with other methods (abstr). *Proceedings of annual meeting Soc Magn Reson Med,* New York, August **1987**:56
24. *Scanning guide for release 3.2 and Performance Plus. 3D volume fast scan.* Milwaukee: General Electric Medical Systems, **1988**
25. Enzmann DR, Rubin JR, Wright A. Cervical spine MR imaging: generating high-signal CSF in sagittal and axial images. *Radiology* **1986**;163: 233–238
26. Bradley WG, Tsuruda JS. MR sequence parameter optimization: an algorithmic approach. *AJR* **1987**;149:815–823

27. Czervionke LF, Czervionke JM, Daniels DL, Haughton VM. Characteristic features of MR truncation artifacts. *AJNR* **1988**;9:815–824
28. Winkler ML, Ortendahl DA, Mills TC, et al. Characteristics of partial flip angle and gradient reversal MR imaging. *Radiology* **1988**;166:17–26
29. Feinberg DA, Crooks LE, Hoenninger JC, et al. Contiguous thin multisection MR imaging by two-dimensional transform techniques. *Radiology* **1986**;158:811–817
30. Wherli FW. *Advanced MR imaging techniques.* Milwaukee: General Electric Medical Systems, **1986**:8–9
31. Kneeland JB, Shimakawa A, Wehrli FW. Effect of intersection spacing on MR image contrast and study time. *Radiology* **1986**;158:819–822
32. Carlson J, Crooks L, Ortendahl D, Kramer DM, Kaufamn L. Signal-to-noise ratio and section thickness in two-dimensional versus three-dimensional Fourier transform imaging. *Radiology* **1988**;166:266–270
33. Frahm J, Hanicke W, Merboldt K-D. Transverse coherence in rapid flash NMR imaging. *J Magn Reson* **1987**;72:307–314
34. Gyngell ML. The application of steady-state free precession in rapid 2DFT NMR imaging: FAST and CE-FAST sequences. *Magn Reson Imaging* **1988**;6:415–419
35. Wood ML, Silver M, Runge VM. Optimization of spoiler gradients in FLASH MRI. *Magn Reson Imaging* **1987**;5:455–463
36. Zur Y, Stokar S, Bendel P. An analysis of fast imaging sequences with steady-state transverse magnetization refocusing. *Magn Reson Med* **1988**;6:175–193
37. Fram EK, Karid JP, Evans A, Shimakawa A, Johnson GA, Herfkins RH. Fast imaging of CSF: the effect of CSF motion (abstr). *Proceedings of annual meeting Soc Magn Reson Med,* New York, August **1987**:314
38. Ludeke KM, Roschmann P, Tischler R. Susceptibility artifacts in NMR imaging. *Mag Reson Imaging* **1985**;3:329–343
39. Young IR, Khenia S, Thomas DGT, et al. Clinical magnetic susceptibility mapping of the brain. *J Comput Assist Tomogr* **1987**;11:2–6
40. Czervionke LF, Daniels DL, Wehrli FW, et al. Magnetic susceptibility artifacts in gradient-recalled echo MR imaging. *AJNR* **1988**;9:1149–1155
41. Young IR, Cox IJ, Bryant DJ, Bydder GM. The benefits of increasing spatial resolution as a means of reducing artifacts due to field inhomogeneities. *Magn Reson Imaging* **1988**;6:585–590
42. Wood ML, Runge VM, Henkelman RM. Overcoming motion in abdominal MR imaging. *AJR* **1988**;150:513–522
43. Breger RK, Czervionke LF, Kass EG, et al. Truncation artifact in MR images of the intervertebral disk. *AJNR* **1988**;9:825–828
44. Wherli, FW. *Advanced MR imaging techniques.* Milwaukee: General Electric Medical Systems, **1986**: 4–5
45. Roemer PB, Edelstein WA, Hickey JS. Self shielded gradient coils (abstr). *Proceedings of annual meeting Soc Magn Reson Med*, Montreal: **1986**: 1067–1068